



Research article

Integrative analysis of immune microenvironment-related CeRNA regulatory axis in gastric cancer

Jie Chen[#], Jinggui Chen[#], Bo Sun, Jianghong Wu* and Chunyan Du*

Department of Gastric Surgery, Fudan University Shanghai Cancer Center, Shanghai 200032, China

* **Correspondence:** Email: t6kby04eng4@sina.com; elite53@163.com; Tel/fax: +86-021-64175590.

* Chunyan Du is the first corresponding author, Jianghong Wu is the second corresponding author.

[#]The authors should be regard as co-first authors.

Abstract: This study aimed to identify significant immune microenvironment-related competing endogenous RNA (CeRNA) regulatory axis in gastric cancer (GC). Analysis of differentially expressed mRNAs (DEmRNAs), miRNAs (DEmiRNAs), and lncRNAs (DElncRNAs) was performed for the microarray datasets. After abundance analysis of immune cell's infiltration, immune-related mRNAs and lncRNAs were obtained. Meanwhile, according to the Pearson correlation coefficient between immune-related mRNAs and lncRNAs, the co-expression mRNA-lncRNA pairs were screened. Furthermore, the target genes of co-existence miRNAs were predicted, and miRNA-lncRNA pairs were identified. Finally, the lncRNA-miRNA and miRNA-mRNA relationship regulated by the same miRNA was screened. Combining with the co-expression relationship between lncRNA and mRNA, the CeRNA network was constructed. In abundance analysis of immune cell's infiltration, a total of eight immune cells were obtained, in addition, 83 immune-related DElncRNAs and 705 immune-related DEmRNAs were screened. KEGG pathway enrichment analysis showed that these mRNAs were mainly involved in PI3K-Akt signaling pathway and human papillomavirus infection, while lncRNA were relevant to gastric acid secretion. A total of 25 miRNAs were significantly associated with immune-related mRNAs, such as hsa-miR-148a-3p, hsa-miR-17-5p, and hsa-miR-25-3p. From the mRNA-miRNA-lncRNA CeRNA network, we observed that AC104389.28—miR-17-5—SMAD5 axis and LINC01133—miR-17-5p—PBLD axis played a crucial role in the development of GC. Furthermore, resting memory CD4 T cells and plasma cells were closely associated with the pathogenesis of GC, and these immune cells might be affected by the key genes. The present study identified key genes that associated with immune microenvironment in GC, providing potential molecular targets for immunotherapy of GC.

Keywords: gastric cancer; immune; competing endogenous RNA; CeRNA regulatory axis; integrative analysis

1. Introduction

Studies have shown that the incidence of gastric cancer (GC) is decreasing worldwide [1]. In 2018, with the emergence of more than 1,000,000 new cases, GC becomes the fifth most common cancer. Besides, GC is regarded as the third leading cause of cancer death with 783,000 deaths in 2018 [2]. For Chinese people, GC continues to be the primary cause of the cancer burden [3]. For the purpose to maximally reduce locoregional recurrence of advanced GC, gastrectomy and dissection of lymph node are the standard surgery for the treatment of GC [4]. Although the serum carbohydrate antigen, pepsinogen, and carcinoembryonic antigen have been used to diagnose GC, the detection rate is only 5% in the early stage due to lack of symptoms [5]. Therefore, the exploration of developmental mechanism and therapeutic targets of GC is imperative.

In cancer development, evading immune surveillance has become a sign of biological competence [6]. In the cancerous tissues, the host immune system can recognize cancer cells and destroy them, suggesting that the evasion of tumor cells from the destruction of the immune system is significant in the process of tumor development [7]. The clinical course of the disease often determined by the ability of the tumor to evade recognition by the immune system [8]. With the discovery of infiltrating immune cells in various malignancies, immune parameters may have significance for the prognosis assessment of cancer patients [9]. Liu et al [10] revealed that immune cells contributed to determining the prognosis of GC, and high TCD68+/SCD68+ ratio and TCD8+/TFoxp3+ ratio were associated with improved overall survival, which were promising independent predictors for overall survival in GC. Additionally, tumor-infiltrating immune cells could be used reinforce the clinical outcome prediction ability of the TNM staging system and provide a convenient tool for treatment selection for patients with GC [11]. However, the relevant bio-molecular mechanisms of the immune microenvironment in GC have not been fully elucidated.

Long non-coding RNA (lncRNA) has been widely investigated in a variety of diseases [12]. Studies have shown that lncRNAs can be regarded as potential therapeutic targets for cancer treatment, which regulate signal transduction pathways involved in tumor proliferation, metastasis, migration, apoptosis, and drug resistance [13–15]. The lncRNA has recently received increasing attention due to its functions as competing endogenous RNA (CeRNA) to hinder miRNA functions that participate in post-transcriptional regulatory networks in tumors, revealing that lncRNA and mRNA can hinder miRNA function by virtue of shared microRNA response elements (MREs) as natural miRNA sponges [16]. Growing evidences have reported the role of CeRNA in the development of cancer. Luan et al [17] reported that lncRNA XLOC_006390 might serve as a CeRNA that reversely regulated the expression of miR-331-3p and miR-338-3p, thus promoting cervical cancer tumorigenesis and metastasis. Additionally, previous study has indicated that CeRNA might serve as diagnostic biomarkers or therapeutic targets for GC [18]. Chen et al [19] revealed that lncRNA LINC01234 contributed to GC by competitively binding with miR-204-5p to regulated core-binding factor subunit beta (CBFB) expression, suggesting these genes might be considered as novel targets for GC diagnosis and therapy. Meanwhile, lncRNA HNF1A-AS1 induced GC progression by competitively binding miR-661 with cell division cycle 34 (CDC34), and provided

that non-coding RNA might promote the progression of GC by regulating the cell cycle [20]. Nevertheless, there remain insufficient comprehensive analyses on the lncRNAs and miRNAs related to GC on the basis of immune cells. In our study, microarray datasets of GC were downloaded from the public database. Then, differentially expressed mRNA (DEmRNA), differentially expressed miRNA (DEmiRNA), and differentially expressed lncRNA (DElncRNA) between GC tissues and control tissues were screened. Meanwhile, immuno-infiltration analysis was conducted to identify the differential immune cell subset between GC tissues and control tissues. The relationship between lncRNA/mRNA and immune cell was analyzed. Besides, the lncRNA-mRNA pairs and miRNA-lncRNA pairs were respectively predicted. Based on these interactions, the immune cell-related mRNA-miRNA-lncRNA CeRNA network was constructed. Importantly, the proposed immune-related network might allow a better understanding of the regulatory mechanism of CeRNA mediated by lncRNA in the pathogenesis and prognosis of GC.

2. Materials and method

2.1. Data source

After a careful review of the Gene Expression Omnibus (GEO, <http://www.ncbi.nlm.nih.gov/geo/>) database [21], we finally selected four microarray datasets (GSE65801, GSE23739, GSE26595, and GSE30073) to screen the differentially expressed genes between GC tissues and normal tissues, and raw data were downloaded in October 2019. The microarray dataset GSE65801 [22] based on GPL14550 Agilent-028004 SurePrint G3 Human GE 8x60K Microarray (Probe Name Version) platform was obtained from GEO database, and composed of the lncRNA/mRNA data of 32 GC tissues and 32 normal tissues. Among these, GC tissues were taken from untreated patients with primary gastric carcinomas, and who underwent D2 radical gastrectomy. Microarray dataset GSE23739 [23] was derived from GPL7731 platform (Agilent-019118 Human miRNA Microarray 2.0 G4470B (Feature Number version)), and contained miRNA expression data of 40 GC tissues and 40 normal tissues. The primary gastric tumors and adjacent normal gastric tissues were obtained from the National Cancer Centre Singapore, Singapore, and the Singhealth Tissue Repository. Microarray dataset GSE26595 [24] based on GPL8179 Illumina Human v2 MicroRNA expression beadchip platform was downloaded from GEO database, and included miRNA data of 60 GC tissues and eight normal tissues. The clinical features of patients in this dataset are listed in Supplementary Table 1. Furthermore, the platform for GSE30073 [25] was GPL13742 Agilent-015868 Human miRNA Microarray (miRBase release 9.0 Feature Number version)], and this dataset contained miRNA expression data of 90 GC samples and 34 normal samples. The clinico-pathological characteristics of patients are shown in Supplementary Table 2.

2.2. Pre-preprocessing of the data

In the expression profile analysis of the mRNA/lncRNA, the processed and standardized probe expression matrix file (GSE65801_series_matrix.txt) was downloaded from the GEO database; meanwhile, all probes sequencing in GPL14550 Agilent-028004 SurePrint G3 Human GE 8x60K Microarray (Probe Name Version) platform were also downloaded, and human reference genome (GRCh38) was obtained from GENCODE [26] database (<https://www.genencode.org/releases/current.html>). All probe sequences were aligned to the reference genome by using seqmap software [27]. Briefly, the uniquemap probes were reserved, then,

using its position on the chromosome and positive and negative strand information, the genes corresponding to each probe were obtained according to the human gene annotation file (Release25). Specifically, reserving the probes with annotation information “protein_coding” as corresponding mRNA probes; while retaining the probes with annotation information "antisense", "sense_intronic", "lincRNA", "sense_overlapping", "3prime_overlapping_ncRNA", "bidirectional_promoter_lincRNA", "macro_lincRNA" or "processed_transcript" as the corresponding lincRNA probes. The probes matching to mRNA/lincRNA (Genesymbol) were retained, while probes that not matching to Genesymbol were removed. The average values of the different probes were selected as the final expression value of mRNA/lincRNA when different probes matching to the same gene.

In the expression profile analysis of miRNA (GSE23739, GSE26595, and GSE30070), the original probe signal value file was downloaded from GEO database, and was preprocessed by using limma [28] package, including background correction, robust multi-array average normalization, and calculation of expression value. Additionally, the annotation file corresponding to platform was downloaded. Firstly, the miRNA ID was mapped to the miRNA version (v22) of the mirBase database (<http://www.mirbase.org/>) [29] to obtain the miRNA name. Then, the probes were mapped to miRNA. The mean value of different probes was considered as the final expression value of miRNA when the multiple probes corresponding to the same miRNA name, while probes without corresponding miRNA name were deleted.

2.3. Differentially expressed analysis

The classical Bayesian method in limma package (Version 3.10.3, <http://www.bioconductor.org/packages/2.9/bioc/html/limma.html>) [28] was applied to perform differential expression analysis, including DE mRNA and DE lincRNA in GSE65801, as well as DE miRNA in GSE23739, GSE26595, and GSE30073. The p value was adjusted by the Benjamini/Hochberg test. The screening threshold of DE mRNA and DE lincRNA was adjusted p value < 0.05 and $|\log \text{fold change (FC)}| > 1$, whereas the adjusted p value < 0.05 and $|\log \text{FC}| > 0.585$ were considered as the thresholds of DE miRNA.

2.4. Abundance analysis of infiltrating immune cells

Based on the gene expression matrix, the algorithm of CIBERSORT deconvolution [30] was utilized to estimate the abundance of immune infiltration. The gene expression feature template was provided by the LM22 dataset of CIBERSORT, which contained 22 immune-related cells. After obtaining the infiltration abundance of 22 types of cells in each sample, the samples with p value < 0.05 were selected. The differentially analysis was conducted by T test to explore the immune-related cells between GC tissues and normal tissues, and p value < 0.05 was considered as statistically significant. Besides, ggplot2 (Version: 3.2.1) in R package was used to constitute the landscape histogram of the abundance of immune cell infiltration. The boxplot in R package (version 0.3.2) was used to constitute the violin plot of differentially infiltrated immune cells.

2.5. Analysis of immune-related mRNA/lincRNA and pathway enrichment of mRNA

Based on the obtained differential immune cells, the cor. test of R language was used to respectively calculate the spearman correlation coefficient between DE mRNA-immune cells and DE lincRNA-immune cells, which conducted with the significance test. The immune-related

mRNAs/lncRNAs were screened out with the threshold of p-value < 0.05 and correlation coefficient $|r| > 0.6$.

Utilizing the ClusterProfiler tool [31] in R package (Version:3.8.1, <http://bioconductor.org/packages/release/bioc/html/clusterProfiler.html>), Kyoto Encyclopedia of Genes and Genomes (KEGG) pathway enrichment analyses was performed for the immune-related DEmRNAs, and p value < 0.05 and count ≥ 2 were defined as the cut-off criteria.

2.6. Co-expression analysis of mRNA/lncRNA and pathway enrichment of lncRNA

Utilizing the cor.test of R language, the Pearson correlation coefficient between the immune-related mRNAs and immune-related lncRNAs was calculated and conducted with the significance test. The threshold value of significantly correlated mRNA-lncRNA pairs was r value > 0.8 and p-value < 0.05 . Cytoscape software (version 3.4.0, <http://chianti.ucsd.edu/cytoscape-3.4.0/>) [31] was applied to structure the co-expressed network of lncRNA-mRNA.

Meanwhile, the mRNAs were served as the potential target genes of lncRNAs, and the KEGG pathway enrichment analysis of mRNA was conducted by using ClusterProfiler in R package. P-value < 0.05 and the number of enriched genes ≥ 2 were considered as significant enrichment results, which indirectly predicted the function of lncRNA.

2.7. Target genes prediction of miRNA and pathway enrichment analysis

The up-regulated miRNAs and down-regulated miRNAs in three sets of GSE23739, GSE26595, and GSE30070 datasets were respectively intersected, and miRNAs with differences in at least two datasets were selected for further analysis. Online tool MiRWalk3.0 [32] (http://mirwalk.umm.uni-heidelberg.de/search_genes/) was used to predict the target genes for the DEmiRNAs. The mRNA that existed at least in TargetScan or miRDB was retained. Then, these genes were overlapped with immune-related mRNA to obtain miRNA-mRNA pairs, and the miRNA-target regulatory network was constructed using Cytoscape software. Similarly, ClusterProfiler was used to conduct KEGG pathway enrichment analysis of the target genes in miRNA-mRNA relationship, which was indirectly defined as the pathway enrichment analysis results of miRNA. The screening threshold of significantly enriched pathways was p-value < 0.05 .

2.8. Analysis of lncRNA-miRNA relationship and construction of CeRNA network

According to the previously obtained immune-related lncRNAs and DEmiRNAs, the Miranda (v3.3a) [33] software (parameters: -sc 140, -en -20), was used to obtain the miRNA-lncRNA relationship. Combined with the miRNA-mRNA pairs, the lncRNA-miRNA-mRNA pairs regulated by the same miRNA were screened. Meanwhile, based on the correlation coefficients > 0.95 of co-expressed lncRNA-mRNA pairs, the lncRNA-miRNA-mRNA pairs were further screened to establish the CeRNA network. Among these, lncRNA and mRNA with positive co-expression relationship regulated by the same miRNA were CeRNA with each other.

3. Results

3.1. Preprocess of the data

In the GSE65801, a total of 42545 probes were downloaded from the platform. Compared to the genome, 32054 probes were obtained. Among these, 5159 lncRNA probes were retained, corresponding to 2870 lncRNA; while 24890 mRNA probes were reserved, corresponding to 16325 mRNA. In the GSE23739, a total of 15744 probes were obtained from the platform, among these, 11570 probes were human miRNA probes, and these probes corresponding to 713 miRNA. In the GSE26595, a total of 1146 miRNA probes were extracted from the platform, which corresponding to 348 miRNA. In the GSE30070, a total of 2296 miRNA probes were obtained, which corresponding to 407 miRNA. Distribution of standardized data showed that the median was roughly on the same horizontal line (Figure 1), which could be used for the further analysis.

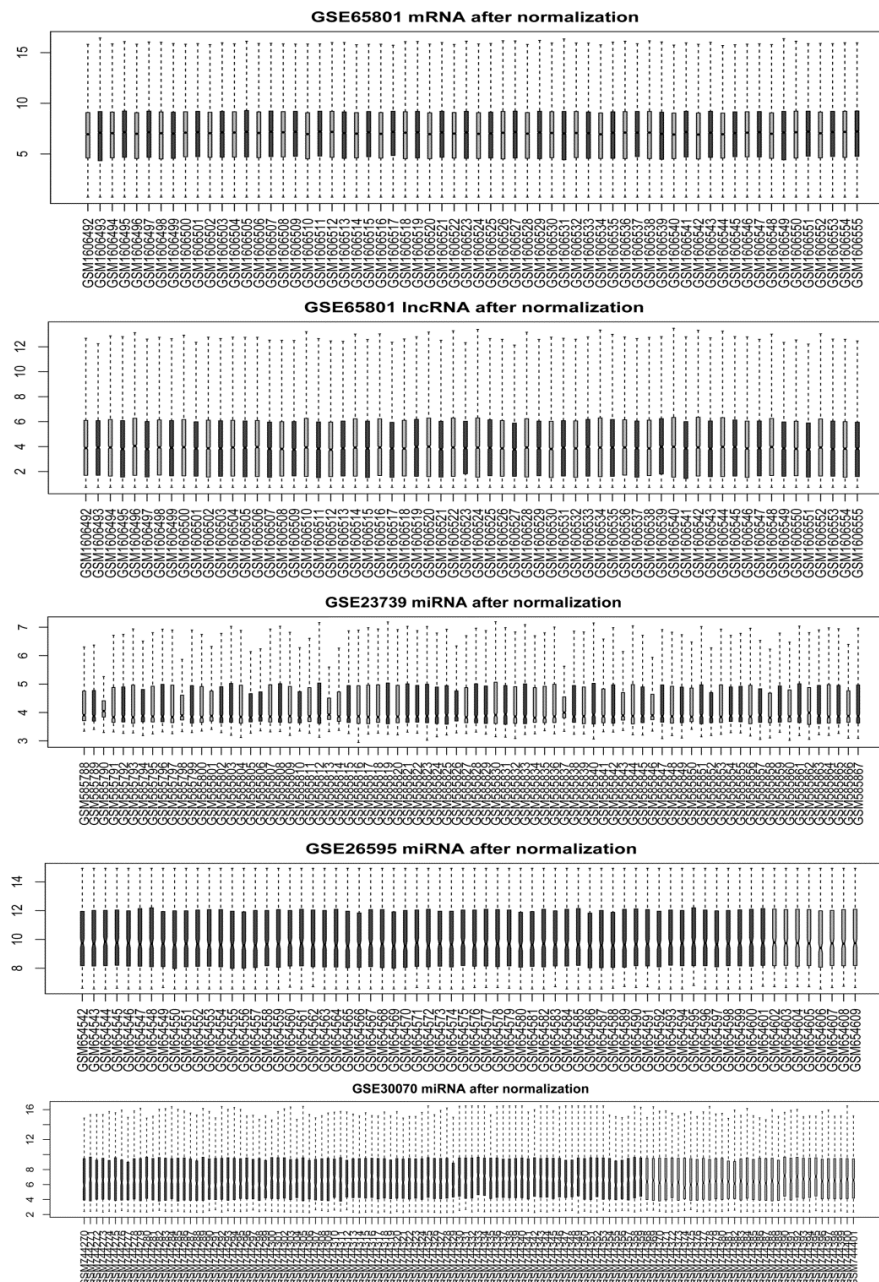


Figure 1. The box diagram of distribution of standardized data. Blue bar represents GC tissues, and yellow bar represents normal tissue.

3.2. Differentially expressed analysis

According to the screening criteria, a total of 1637 DEmRNAs (868 up-regulated and 769 down-regulated) and 218 DElncRNAs (81 up-regulated and 137 down-regulated) were identified in GSE65801; total 218 DEmiRNAs, including 104 DEmiRNAs (60 up-regulated and 44 down-regulated) in GSE23739, 62 DEmiRNAs (34 up-regulated and 28 down-regulated) in GSE26595, and 52 DEmiRNAs (27 up-regulated and 25 down-regulated) in GSE30070, were screened between GC tissues and normal tissues. The bidirectional clustering heatmap (Figure 2) and volcano map (Figure 3) of DEmRNA, DElncRNA, and miRNAs were displayed.

3.3. Abundance analysis of immune cell infiltration

According to the screening threshold, a total of 48 samples (24 tumor samples and 24 normal samples) were selected for the analysis of infiltrating abundance. The histograms of abundance of immune cell infiltration in each sample are shown in Figure 4A. Meanwhile, eight types of immune cells, including plasma cells, naive CD4 T cells, CD8 T cells, gamma delta T cells, resting memory CD4 T cells, M0 Macrophages, M2 Macrophages, and activated dendritic cells, had significantly differential infiltration between tumor and normal tissues (Figure 4B).

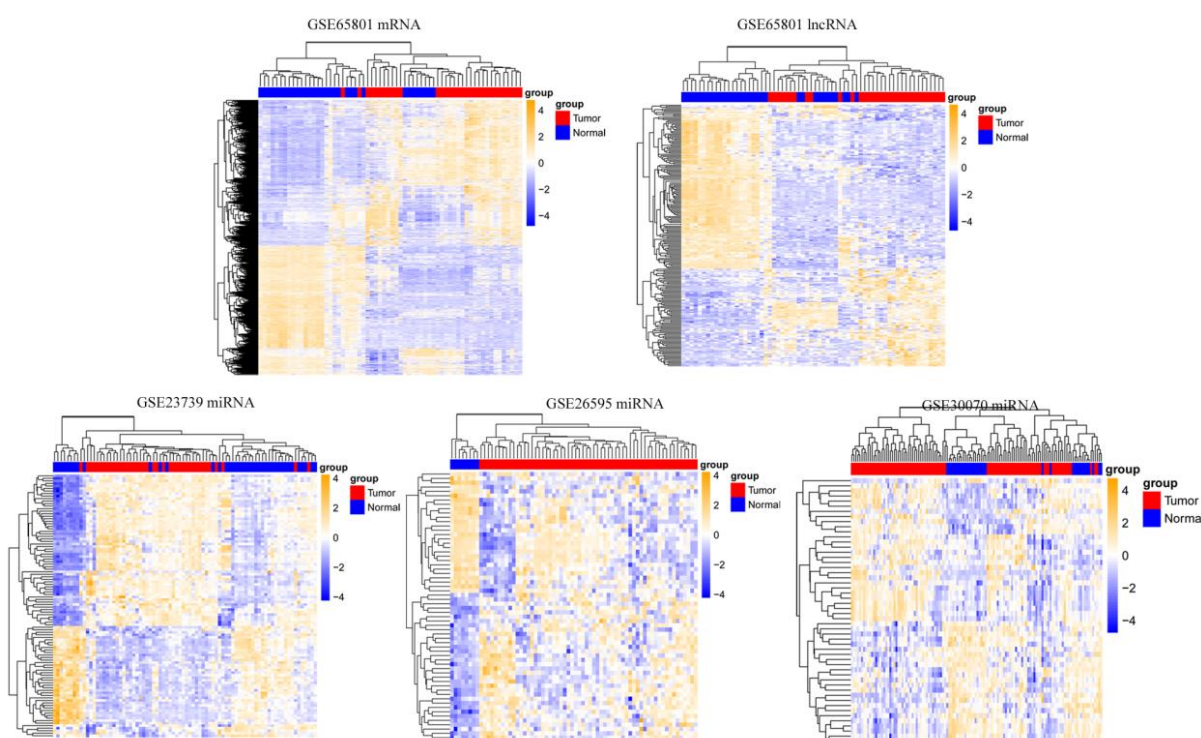


Figure 2. The heat map of differentially expressed mRNAs, lncRNAs and miRNAs. Red indicates tumor sample, and blue indicates normal sample.

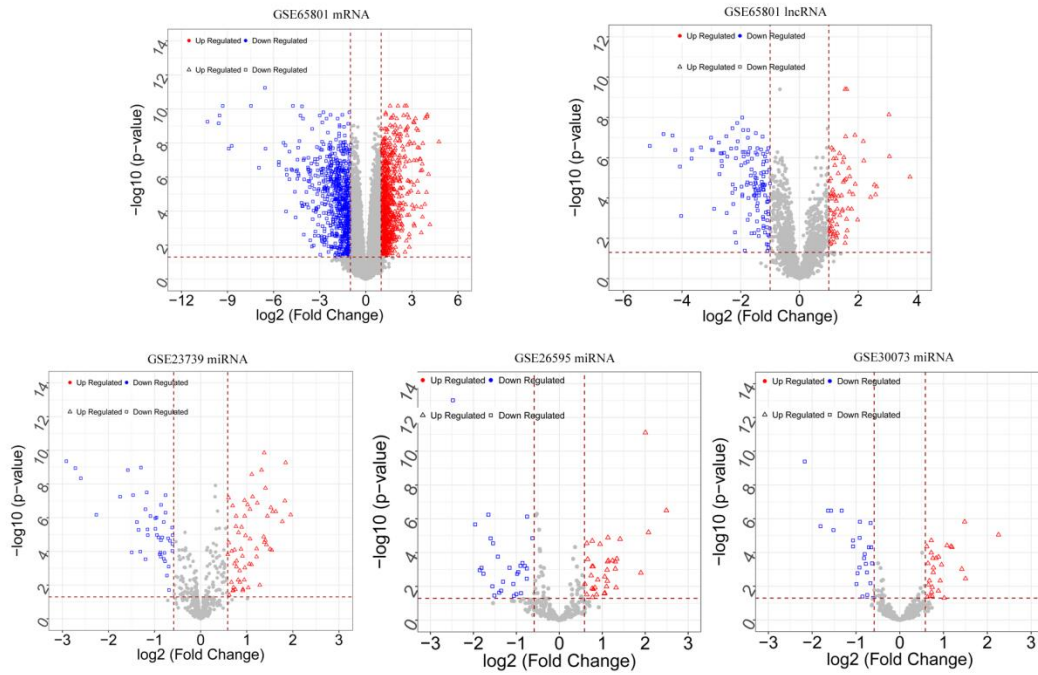


Figure 3. Volcano plot of differentially expressed mRNAs, lncRNAs, and miRNAs. The blue square represents down-regulated gene, the red triangle represents up-regulated gene, and the grey node represents non-significant.

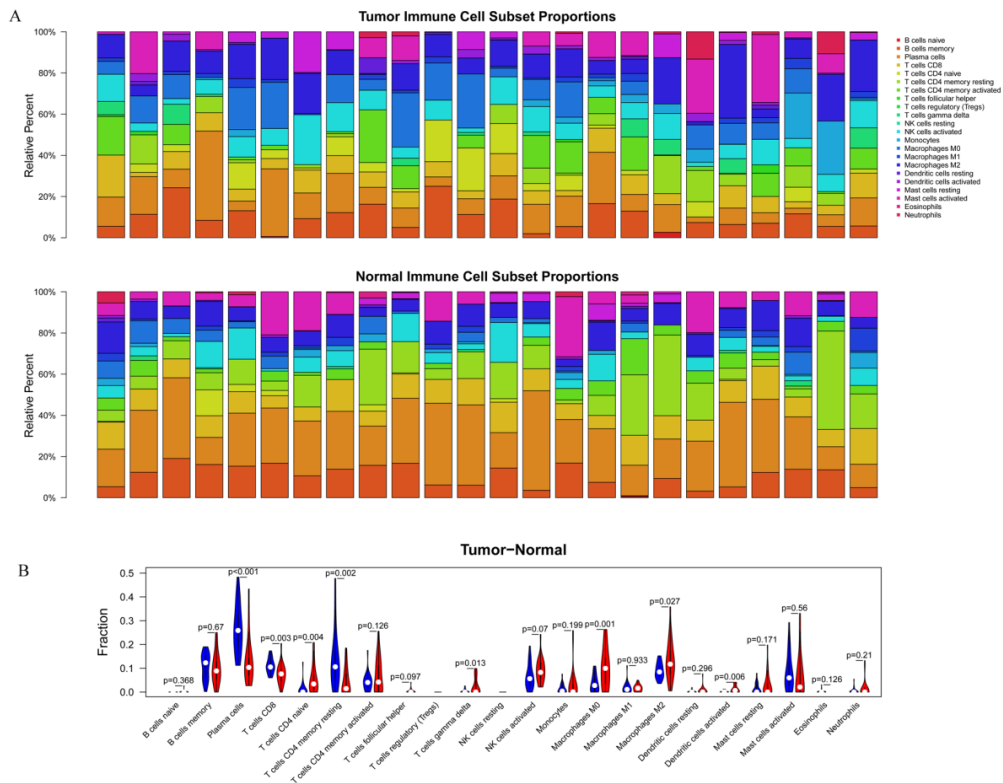


Figure 4. (A) The landscape histogram of infiltrating abundance of immune cell. (B) Violin plot for comparing cells' proportion between the gastric cancer tissues and control tissues.

3.4. Analysis of immune-related mRNA/lncRNA and pathway enrichment of mRNA

Correlation analysis was conducted between mRNA/lncRNA with eight immune cells. According to the threshold, a total of 83 immune-related lncRNAs and 705 immune-related mRNAs were screened. KEGG pathway enrichment analysis of 705 immune-related mRNA showed that a total of 33 pathways were obtained (Figure 5). These mRNAs were mainly involved in pathways such as PI3K-Akt signaling pathway, human papillomavirus infection, and Neuroactive ligand-receptor interaction.

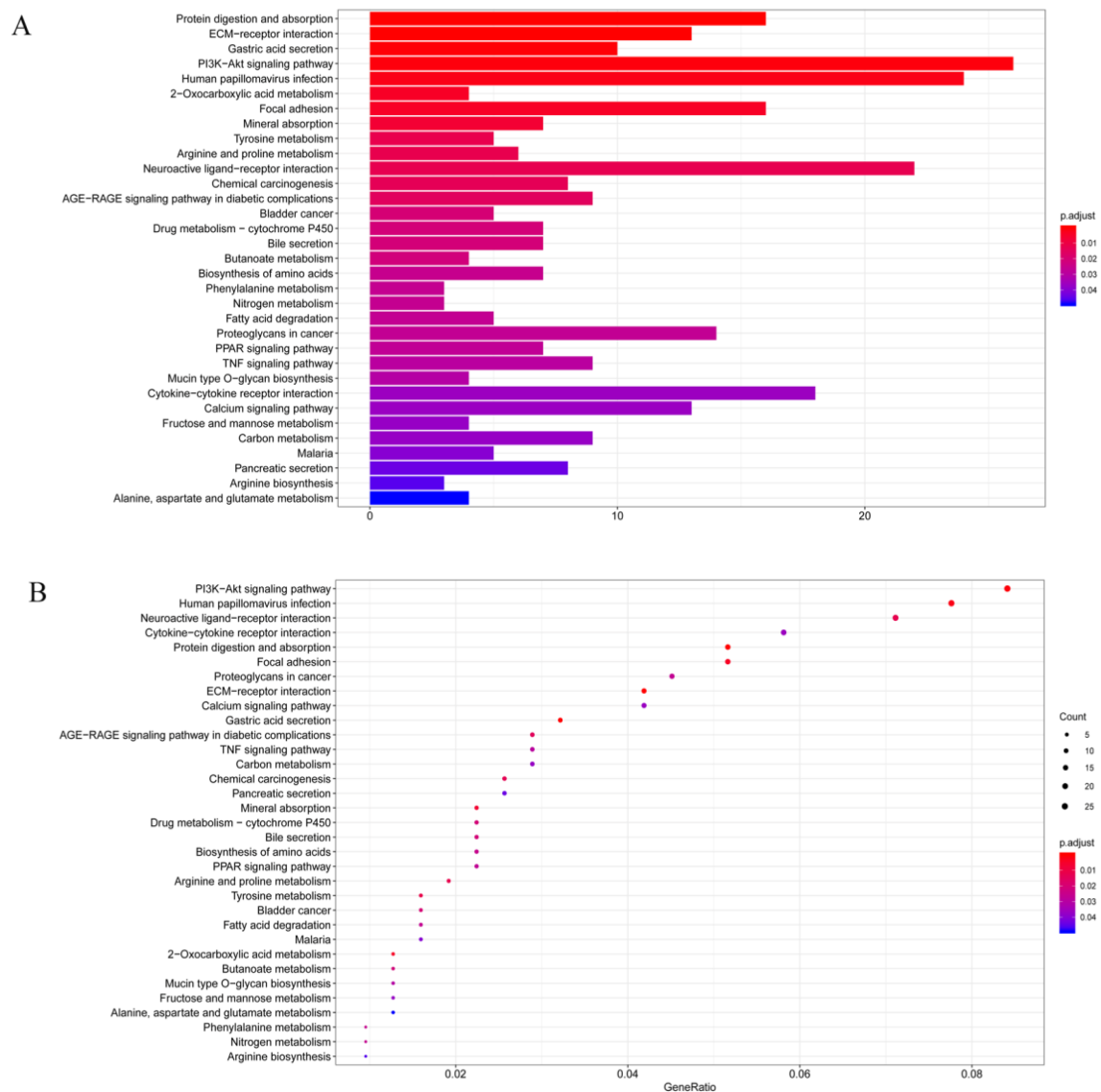


Figure 5. KEGG pathway enrichment analysis of immune-related mRNA. (A) The bar chart of immune-related mRNAs. The abscissa represents the number of enriched genes. (B) The bubble diagram of immune-related mRNAs. The abscissa represents the ratio of enriched genes/background genes in a certain pathway.

3.5. Co-expression analysis of mRNA/lncRNA and pathway enrichment of lncRNA

The co-expression of DEmRNA and DELncRNA was performed, a total of 3558 significantly co-expression mRNA-lncRNA pairs, 432 DEmRNAs, and 72 DELncRNAs were obtained. The network of co-expressed mRNA-lncRNA pairs with Pearson correlation > 0.9 is displayed in Figure 6A.

KEGG pathway enrichment analysis was performed on target genes of 72 lncRNAs. According to the threshold, 49 enriched pathways were obtained. As shown in Figure 6B, the top 10 enrichment pathways were exhibited. These lncRNA primarily participated in gastric acid secretion, tyrosine metabolism, collecting duct acid secretion, and drug metabolism-cytochrome P450.

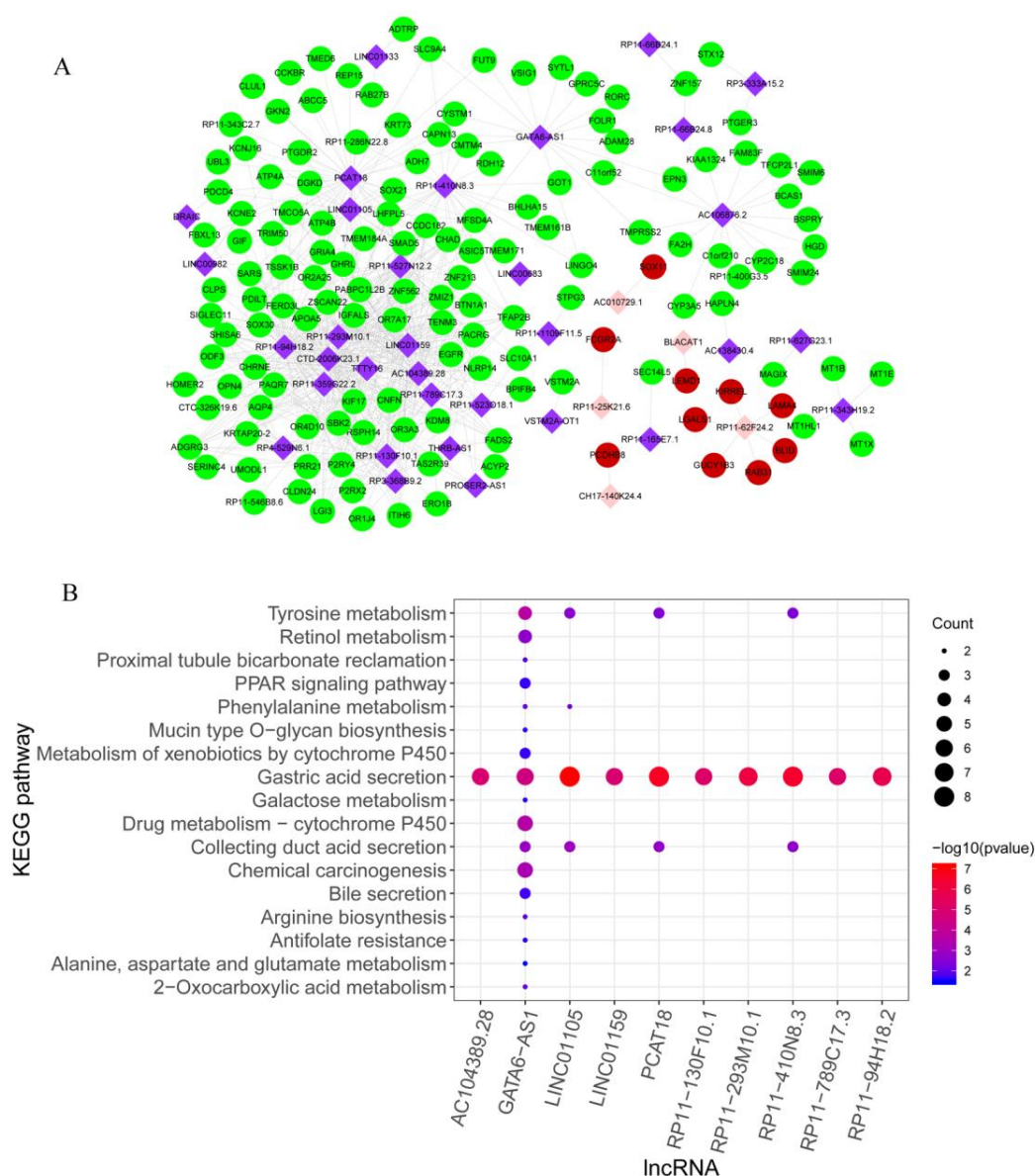


Figure 6. (A) The co-expression analysis of DEmRNAs and DELncRNAs. Red circle represents up-regulated mRNA, green circle represents down-regulated mRNA, pink diamond represents up-regulated lncRNA, and purple diamond represents down-regulated lncRNA. (B) KEGG pathway enrichment analysis of lncRNA in the co-expressed analysis.

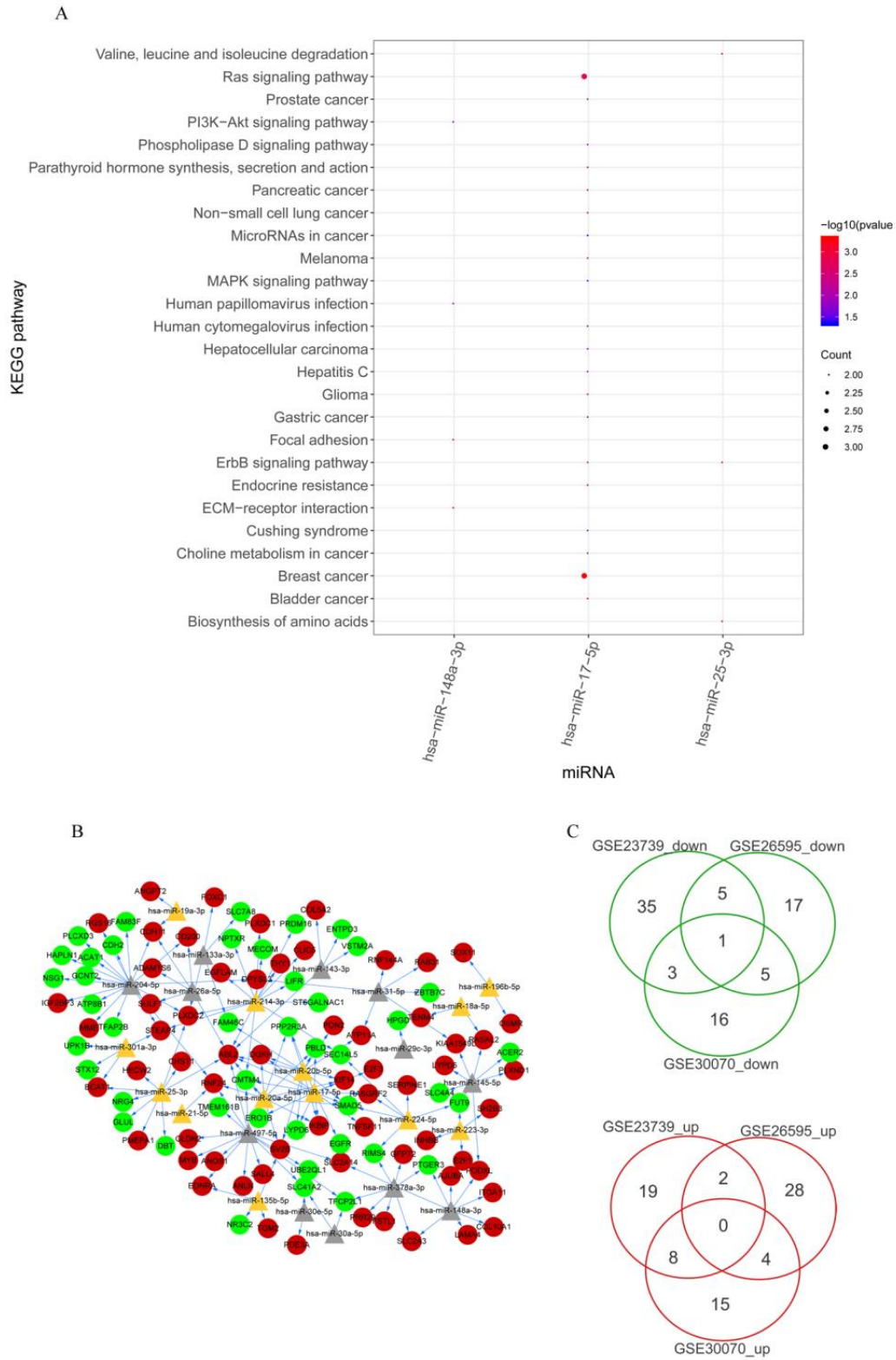


Figure 7. (A) KEGG pathway enrichment analysis of miRNA. (B) The network of DE miRNAs-DE mRNAs. Red circle represents up-regulated mRNAs, green circle represents down-regulated mRNA, yellow triangle represents up-regulated miRNAs, gray triangle represents down-regulated miRNAs. (C) The intersection analysis of DE miRNA in three databases.

3.6. Target genes prediction of miRNA and pathway enrichment analysis

According to the intersection analysis, there were 28 miRNA (14 up-regulated, 14 down-regulated) were selected at least in two databases (Figure 7C). The mirwalk3.0 was used to predict the target genes of 28 miRNAs, and 4088 miRNA-mRNA relationships were obtained. Through an intersection analysis of 705 immune-related mRNAs, 163 miRNA-mRNA pairs (25 miRNAs and 106 mRNAs) were finally obtained (Figure 7B). Besides, KEGG pathway enrichment analysis of 25 miRNAs was performed, the enrichment pathways of 3 miRNA (hsa-miR-148a-3p, hsa-miR-17-5p, and hsa-miR-25-3p) are shown in Figure 7A. Among these, hsa-miR-17-5p was principally involved in ras signaling pathway and breast cancer pathways.

3.7. Analysis of lncRNA-miRNA relationship and construction of CeRNA network

A total of 576 lncRNA-miRNA relationship pairs were predicted which composed of 69 lncRNAs and 27 miRNAs. Finally, a number of 206 lncRNA-miRNA-mRNA relationships were obtained that contained 135 lncRNA-miRNA pairs, 47 miRNA-mRNA pairs, and 122 lncRNA-mRNA relationships. Meanwhile, Cytoscape was used to construct the CeRNA network, which consisted of 15 miRNAs, 27 mRNAs, and 35 lncRNAs (Figure 8). Among these, several mRNAs targeted by hsa-miR-17-5p, such as epidermal growth factor receptor (EGFR), E2F transcription factor 3 (E2F3), phenazine biosynthesis like protein domain containing (PBLD), and SMAD Family Member 5 (SMAD5). Moreover, lncRNAs such as LINC00534 (degree = 24), DRAIC (degree = 20), and AC104389.28 (degree = 18) with higher degrees, and might be considered as hub nodes.

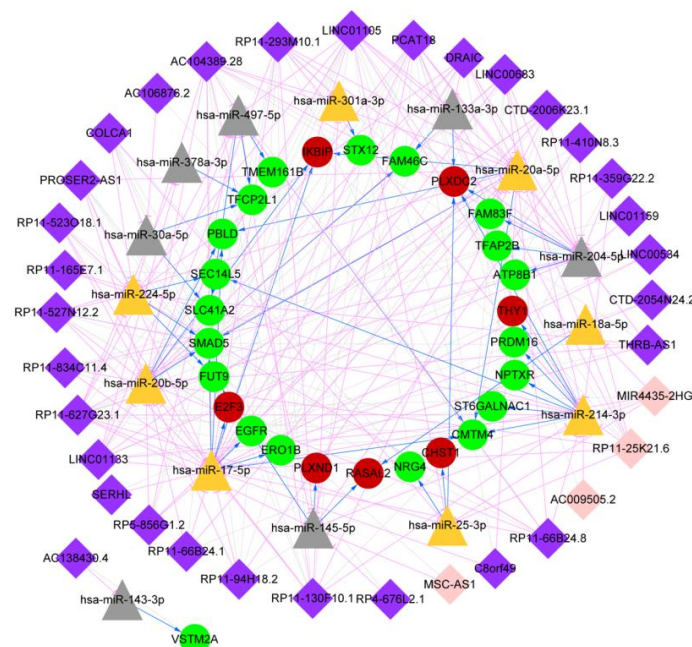


Figure 8. The CeRNA network. Red circle represents up-regulated mRNAs, green circle represents down-regulated mRNA, yellow triangle represents up-regulated miRNAs, gray triangle represents down-regulated miRNAs, pink diamond represents up-regulated lncRNA, purple diamond represents down-regulated lncRNA.

4. Discussion

Despite the decreased incidence of GC, the prognosis of GC remains poor. Recently, the introduction of modern immunotherapy, especially the use of immune checkpoint inhibitors, has improved the prognosis of many types of cancers [34]. Therefore, understanding the complex relationship between host's immune microenvironment and tumors, as well as the immune-related molecular mechanisms that lead to development and progression of tumor will be helpful to identify prognostic immune markers. In this study, we found eight types of immune cells were closely associated with the development of GC, such as CD8 T cells, naïve CD4 T cells, resting memory CD4 T cells, gamma delta T cells, M0 Macrophages, and M2 Macrophages. A total of 83 immune-related lncRNAs and 705 immune-related mRNAs were obtained. KEGG pathway enrichment analysis showed that these mRNAs were mainly involved in PI3K-Akt signaling pathway and human papillomavirus infection, while lncRNA were relevant to gastric acid secretion. Meanwhile, 25 miRNAs were significantly associated with immune-related mRNAs, such as hsa-miR-148a-3p, hsa-miR-17-5p, and hsa-miR-25-3p. From the mRNA-miRNA-lncRNA CeRNA network, we observed that AC104389.28—miR-17-5—SMAD5 axis and LINC01133—miR-17-5p—PBLD axis played crucial roles in the development of GC.

Drosophila mothers against decapentaplegic (SMADs) gene had three subclasses, [receptor-regulated SMADs (R-SMADs), common mediator SMADs, and inhibitory SMADs], which had been found in mammals [35]. R-SMADs could be subdivided into two subtypes according to the process of phosphorylation, which could be generated by transforming growth factor-beta or by bone morphogenetic protein. Via probably up-regulated R-SMADs (SMADs1, 5, 8), BMP mediated apoptosis actively in the limb of embryonic [36]. The study also showed that SMAD5 was mediated apoptosis of gastric epithelial cells caused by *H. pylori* infection [37]. In GC cells, apoptosis was generally inhibited, although proliferation was still accelerating [37]. MiR-17-5p was belonged to miR-17-92 cluster [38]. Compared with normal tissues, the expression level of miR-17-5p was higher in pancreatic cancer, colorectal cancer, glioma, hepatocellular carcinoma, basal cell carcinoma, and GC [38]. By targeting p21 and tumor protein p53-induced nuclear protein 1 (TP53INP1), lack of miR-17-5p would influence the growth of AGS cells, in which cell cycle was arrested and apoptosis was increased. Whereas overexpression of miR-17-5p promoted the progression of cell cycle and inhibited the apoptosis of GC cells [39]. In our study, SMAD5 was down-regulated, while miR-17-5p was up-regulated in GC tissues compared with control tissues. Meanwhile, miR-17-5p was bound to lncRNA AC104389.28. Moreover, we observed that SMAD5 and AC104389.28 were associated with the resting memory CD4 T cells. Rohr-Udilova and colleague [40] reported the relationship between resting memory CD4 T cells and hepatocellular carcinoma (HCC), indicating the number of this immune cell was increased in HCC tissues compared with health tissues. Furthermore, Jiang et al [41] showed that resting memory CD4 T cells were relevant to the prognosis of GC, and it was significantly higher in the high-risk group compared with the low-risk group. Taken together, a hypothesis was presented that AC104389.28 might function as a CeRNA in regulating SMAD5 expression of GC through competitively binding to miR17-5p, and SMAD5 played important role in the development of GC by affecting the number of resting memory CD4 T cells.

PBLD, also termed as mitogen-activated protein kinase activator with WD-40 repeats (MAWD) binding protein, was identified from a human liver cDNA library firstly [42]. The transcription activated by TGF- β was inhibited by MAWD, which contributed to protein/protein interactions [43].

More recently, the study proved that down-regulated PBLD could cause gastric carcinogenesis [44]. Through inhibiting TGF- β 1-induced Epithelial-Mesenchymal Transition (EMT), the growth and invasion in GC cell-lines were negatively regulated by PBLD [43]. Meanwhile, the previous study showed that miR-17-5p had a pro-proliferative function in the development of cancer cells which was highly regulated in GC tissues [45]. In this study, miR-17-5p was regulated by lncRNA LINC01133. We also found both PBLD and LINC01133 were connected with plasma cells. Plasma cells provided protective immunity against recurring sources of infection [46]. Previous study found that multiple myeloma was characterized by the cloning and amplification of malignant plasma cells [47]. Although there was no literature directly reported the relationship between plasma cells and GC, the role of plasma cells in the development of cancer cannot be ignored. Therefore, we predicted that LINC01133 might function as a CeRNA in regulating PBLD expression of GC through competitively binding to miR-17-5p, and these genes might affect the plasma cells in GC tissues.

5. Conclusion

In conclusion, a series of bioinformatics analyses were conducted with immune microenvironment in GC patients. Several CeRNA mechanisms were proposed in this study. AC104389.28 might function as a CeRNA in regulating SMAD5 expression through competitively binding to miR-17-5p. Meanwhile, LINC01133 might affect the expression of PBLD with the competitively binding to miR-17-5p. However, these results should be validated and supported by further experimental studies.

Acknowledgements

This work was supported by The National Natural Science Foundation of China (NSFC) (Program No. 81702356) .

Conflict of interest

The authors declare that they have no competing interests.

References

1. W. Tarupi, E. de Vries, P. Cueva, J. Yépez, Stagnation in decreasing gastric cancer incidence and mortality in quito: Time trend analysis, 1985–2013, *J. Cancer Epidemiol.*, **2019** (2019), 1–10.
2. F. Bray, J. Ferlay, I. Soerjomataram, R. L Siegel, L. A Torre, A. Jemal, Global cancer statistics 2018: GLOBOCAN estimates of incidence and mortality worldwide for 36 cancers in 185 countries, *CA Cancer J. Clin.*, **68** (2018), 394–424.
3. L. Yang, R. Zheng, N. Wang, Y. Yuan, S. Liu, H. Li, et al., Incidence and mortality of stomach cancer in China, 2014, *Chinese J. Cancer Res.*, **30** (2018), 291–298.
4. Japanese Gastric Cancer Association, Japanese gastric cancer treatment guidelines 2014 (ver. 4), *Gastric Cancer*, **20** (2017), 1–19.
5. C. Hamashima, Current issues and future perspectives of gastric cancer screening, *World J. Gastroentero.*, **20** (2014), 13767–13774.
6. C. Mascaux, M. Angelova, A. Vasaturo, J. Beane, K. Hijazi, G. Anthoine, et al., Immune evasion

- before tumour invasion in early lung squamous carcinogenesis, *Nature*, **571** (2019), 570–575.
7. G. Klein, E. Klein, Surveillance against tumors--is it mainly immunological?, *Immunol. Lett.*, **100** (2005), 29–33.
 8. L. Hoenicke, L. Zender, Immune surveillance of senescent cells—biological significance in cancer- and non-cancer pathologies, *Carcinogenesis*, **33** (2012), 1123–1126.
 9. O. Nakano, M. Sato, Y. Naito, K. Suzuki, S. Orikasa, M. Aizawa, et al., Proliferative activity of intratumoral CD8(+) T-lymphocytes as a prognostic factor in human renal cell carcinoma: clinicopathologic demonstration of antitumor immunity, *Cancer Res.*, **61** (2001), 5132–5136.
 10. K. Liu, K. Yang, B. Wu, H. Chen, X. Chen, L. Jiang, et al., Tumor-infiltrating immune cells are associated with prognosis of gastric cancer, *Medicine (Baltimore)*, **94** (2015), e1631.
 11. L. Li, Y. Ouyang, W. Wang, D. Hou, Y. Zhu, The landscape and prognostic value of tumor-infiltrating immune cells in gastric cancer, *Peer J.*, **7** (2019), e7993.
 12. C. P. Ponting, P. L. Oliver, W. Reik, Evolution and Functions of Long Noncoding RNAs, *Cell*, **136** (2009), 629–641.
 13. Y. Gu, T. Chen, G. Li, X. Yu, Y. Lu, H. Wang, et al., LncRNAs: Emerging biomarkers in gastric cancer, *Future Oncol.*, **11** (2015), 2427–2441.
 14. Y. Qi, H. S. Ooi, J. Wu, J. Chen, X. Zhang, S. Tan, et al., MALAT1 long ncRNA promotes gastric cancer metastasis by suppressing PCDH10, *Oncotarget*, **7** (2016), 12693–12703.
 15. M. Qiu, Y. Xu, X. Yang, J. Wang, J. Hu, L. Xu, et al., CCAT2 is a lung adenocarcinoma-specific long non-coding RNA and promotes invasion of non-small cell lung cancer, *Tumor Biol.*, **35** (2014), 5375–5380.
 16. J. Long, J. Xiong, Y. Bai, J. Mao, J. Lin, W. Xu, et al., Construction and Investigation of a lncRNA-Associated ceRNA Regulatory Network in Cholangiocarcinoma, *Front Oncol.*, **9** (2019), 649.
 17. X. Luan, Y. Wang, LncRNA XLOC_006390 facilitates cervical cancer tumorigenesis and metastasis as a ceRNA against miR-331-3p and miR-338-3p, *J. Gynecol. Oncol.*, **29** (2018), e95.
 18. X. Qi, D. H. Zhang, N. Wu, J. Xiao, X. Wang, W. Ma, ceRNA in cancer: Possible functions and clinical implications, *J. Med. Genet.*, **52** (2015), 710–718.
 19. X. Chen, Z. Chen, S. Yu, F. Nie, S. Yan, P. Ma, et al., Long noncoding RNA LINC01234 functions as a competing endogenous RNA to regulate CBFβ expression by sponging miR-204-5p in gastric cancer, *Clin. Cancer Res.*, **24** (2018), 2002–2014.
 20. H. Liu, S. Liu, L. Liu, R. Ma, P. Gao, EGR1-mediated transcription of lncRNA-HNF1A-AS1 promotes cell-cycle progression in gastric cancer, *Cancer Res.*, **78** (2018), 5877–5890.
 21. T. Barrett, R. Edgar, Mining microarray data at NCBI's gene expression omnibus (GEO)*, *Methods Mol. Biol.*, **338** (2006), 175–190.
 22. H. Li, B. Yu, J. Li, L. Su, M. Yan, J. Zhang, et al., Characterization of differentially expressed genes involved in pathways associated with gastric cancer, *PLoS One*, **10** (2015), e0125013.
 23. H. K. Oh, A. L. Tan, K. Das, C. H. Ooi, N. T. Deng, I. B. Tan, et al., Genomic loss of miR-486 regulates tumor progression and the OLFM4 antiapoptotic factor in gastric cancer, *Clin. Cancer Res.*, **17** (2011), 2657–2667.
 24. J. Y. Lim, S. O. Yoon, S. Y. Seol, S. W. Hong, J. W. Kim, S. H. Choi, et al., Overexpression of miR-196b and HOXA10 characterize a poor-prognosis gastric cancer subtype, *World J. Gastroenterol.*, **19** (2013), 7078–7088.
 25. C. H. Kim, H. K. Kim, R. L. Rettig, J. Kim, E. Lee, O. Aprelikova, et al., miRNA signature

- associated with outcome of gastric cancer patients following chemotherapy, *BMC Med. Genom.*, **4** (2011), 79.
26. J. Harrow, F. Denoeud, A. Frankish, A. Raymond, C. K. Chen, J. Chrast, et al., GENCODE: Producing a reference annotation for ENCODE, *Genome Biol.*, **7** (2006), S4.1–9.
 27. H. Jiang and W. H. Wong, SeqMap: Mapping massive amount of oligonucleotides to the genome, *Bioinformatics*, **24** (2008), 2395–2396.
 28. G. K. Smyth, Limma: Linear Models for Microarray Data, in: *Bioinformatics and computational biology solutions using R and Bioconductor* (eds. R. Gentleman and V. J. Carey), Springer, (2005), 397–420.
 29. S. Griffiths-Jones, miRBase: MicroRNA sequences and annotation, *Curr. Protoc. Bioinform.*, **29** (2010), 12.9.1–10.
 30. B. Chen, M. S. Khodadoust, C. L. Liu, A. M. Newman, A. A. Alizadeh, Profiling tumor infiltrating immune cells with CIBERSORT, *Methods Mol. Biol.*, **1711** (2018), 243–259.
 31. G. Yu, L. Wang, Y. Han, Q. He, clusterProfiler: An R package for comparing biological themes among gene clusters, *Omics J. Integrat. Biol.*, **16** (2012), 284–287.
 32. H. Dweep, C. Sticht, P. Pandey, N. Gretz, miRWalk-Database: Prediction of possible miRNA binding sites by “walking” the genes of three genomes, *J. Biomed. Inform.*, **44** (2011), 839–847.
 33. A. J. Enright, B. John, U. Gaul, T. Tuschl, C. Sander, D. S. Marks, MicroRNA targets in *Drosophila*, *Genome Biol.*, **5** (2003), R1.
 34. D. C. Lazăr, M. F. Avram, I. Romoșan, M. Cornianu, S. Tăban, A. Goldiș, Prognostic significance of tumor immune microenvironment and immunotherapy: Novel insights and future perspectives in gastric cancer, *World J. Gastroentero.*, **24** (2018), 3583–3616.
 35. S. Cascio, A. D'Andrea, R. Ferla, E. Surmacz, E. Gulotta, V. Amodeo, et al., miR-20b modulates VEGF expression by targeting HIF-1 α and STAT3 in MCF-7 breast cancer cells, *J. Cell. Physiol.*, **224** (2010), 242–249.
 36. A. R. Hallahan, J. I. Pritchard, R. A. S. Chandraratna, R. G. Ellenbogen, J. R. Geyer, R. P. Overland, et al., BMP-2 mediates retinoid-induced apoptosis in medulloblastoma cells through a paracrine effect, *Nat. Med.*, **9** (2003), 1033–1038.
 37. T. Nagasako, T. Sugiyama, T. Mizushima, Y. Miura, M. Kato, M. Asaka, Up-regulated Smad5 Mediates Apoptosis of Gastric Epithelial Cells Induced by Helicobacter pylori Infection, *J. Biol. Chem.*, **278** (2003), 4821–4825.
 38. Z. Kanaan, H. Roberts, M. R. Eichenberger, A. Billeter, G. Ocheretner, J. Pan, et al., A plasma microRNA panel for detection of colorectal adenomas a step toward more precise screening for colorectal cancer, *Ann. Surg.*, **258** (2013), 400–408.
 39. M. Wang, H. Gu, H. Qian, W. Zhu, C. Zhao, X. Zhang, et al., miR-17-5p/20a are important markers for gastric cancer and murine double minute 2 participates in their functional regulation, *Eur. J. Cancer*, **49** (2013), 2010–2021.
 40. N. Rohr-Udilova, F. Klingmüller, R. Schulte-Hermann, J. Stift, M. Herac, M. Salzman, et al., Deviations of the immune cell landscape between healthy liver and hepatocellular carcinoma, *Sci. Rep.*, **8** (2018), 6220.
 41. B. Jiang, Q. Sun, Y. Tong, Y. Wang, H. Ma, X. Xia, et al., An immune-related gene signature predicts prognosis of gastric cancer, *Medicine (Baltimore)*, **98** (2019), e16273.
 42. C. Iriyama, S. Matsuda, R. Katsumata, M. Hamaguchi, Cloning and sequencing of a novel human gene which encodes a putative hydroxylase, *J. Hum. Genet.*, **46** (2001), 289–292.

43. D. Li, J. Zhang, W. Li, J. Cui, Y. Pan, S. Liu, et al., MAWBP and MAWD inhibit proliferation and invasion in gastric cancer, *World J. Gastroentero.*, **19** (2013), 2781–2792.
44. J. Zhang, B. Kang, X. Tan, Z. Bai, Y. Liang, R. Xing, et al., Comparative analysis of the protein profiles from primary gastric tumors and their adjacent regions: MAWBP could be a new protein candidate involved in gastric cancer, *J. Proteome Res.*, **6** (2007), 4423–4432.
45. Q. Wu, G. Luo, Z. Yang, F. Zhu, Y. An, Y. Shi, et al., miR-17-5p promotes proliferation by targeting SOCS6 in gastric cancer cells, *FEBS Lett.*, **588** (2014), 2055–2062.
46. M. Seifert, R. Küppers, Human memory B cells, *Leukemia*, **30** (2016), 2283–2292.
47. N. Hosen, Multiple myeloma-initiating cells, *Int. J. Hematol.*, **97** (2013), 306–312.

Supplementary

Supplementary Table 1. The clinical features of patients in the GSE26595 n (%).

Characteristic	Group 1 (n = 60)	miR-196b high (n = 28)	miR-196b low (n = 29)	P value	HOXA10 high (n = 29)	HOXA10 low (n = 28)	P value
Age, yr							
Median (range)	63 (32–83)	66 (34–78)	58 (32–83)	0.134	64 (34–83)	60 (32–78)	0.134
>65		15 (52)	9 (32)		15 (52)	9 (32)	
Sex							
Male	41 (68)	19 (68)	20 (69)	0.928	18 (62)	21 (75)	0.294
Histologic type							
Diffuse	27 (45)	9	17	0.066	8	18	0.007
Intestinal	23 (38)	14	9		16	7	
Mixed	10 (17)	5	3		5	3	
T stage							
T1/T2	26 (43)	10 (36)	14 (48)	0.337	11 (38)	13 (46)	0.516
T3/T4	34 (57)	18 (64)	15 (52)		18 (62)	15 (54)	
N stage							
N0/N1	36 (60)	15 (54)	19 (66)	0.358	16 (55)	18 (64)	0.483
N2/N3	24 (40)	13 (46)	10 (34)		13 (45)	10 (36)	
AJCC stage ¹							
I/II	23 (38)	11 (39)	12 (41)	0.872	11 (38)	12 (43)	0.705
III/IV	37 (62)	17 (61)	17 (59)		18 (62)	16 (57)	

¹. Based on the American Joint Committee on Cancer staging manual 6th edition. HOXA10: Homeobox A10; AJCC: American Joint Committee on Cancer.

Supplementary Table 2. Clinico-pathological characteristics of patients in the GSE30070.

	Gastric cancer patient Training set	Proof-of-principle test set (responder)	Healthy volunteer
Number	82	8	34
Age - yr			
Median	56	56	48
Interquartile range	(44–63)	(44–58)	(43–57)
Sex - no. (%)			
Male	64 (78.0%)	7 (87.5%)	23 (67.6%)
Female	18 (22.0%)	1 (12.5%)	11 (32.4%)
Performance status (PS) - no. (%)			
ECOG ¹ PS 0 or 1	73 (89.0%)	8 (100%)	
ECOG PS 2 or 3	9 (11.0%)	0	
Lauren's intestinal	34 (41.5%)	3 (37.5%)	
Lauren's diffuse	48 (58.5%)	5 (62.5%)	
Location of primary lesion - no. (%)			
Upper 1/3	11 (13.4%)	1 (12.5%)	
Middle 1/3	18 (22.0%)	5 (62.5%)	
Lower 1/3	43 (52.4%)	1 (12.5%)	
Entire stomach	10 (12.2%)	1 (12.5%)	
Chemotherapy regimen - no. (%)			
Cisplatin/Fluorouracil	80 (97.6%)	8 (100%)	
Cisplatin/Capecitabine	2 (2.4%)	0	
*Relative dose intensity - %			
Median	81.2	76.6	
Interquartile range	(75.3–87.3)	(64.7-84.9)	
Number of chemotherapy cycles			
Median	4	10	
Interquartile range	(2–5)	(7–11)	
Chemotherapy response (WHO criteria) -no (%)			
PR ²	16 (24.6%)	6 (100%)	
SD ³	25 (38.5%)		
PD ⁴	24 (36.9%)		
Unmeasurable	16	2	
Unevaluable	1		
Second-line chemotherapy	55 (67.1%)	6 (75.0%)	
Median follow-up for survivors	35.5 months	-	
Overall survival - mo.			
Median	8.2	16	
Interquartile range	(6.8-10.5)	(11.3-26.7)	
Time to progression - mo.			
Median	3.1	8.2	
Interquartile range	(2.5–3.9)	(4.3–21.2)	

¹Eastern Cooperative Oncology Group, ²partial response, ³stable disease, ⁴progressive disease.

*Relative dose intensity

*Mean of relative dose intensities of cisplatin and fluorouracil. Dose intensity is defined as the amount of drug administered per unit of time, expressed as milligrams per square meter per week. Relative dose intensity is defined as the actual dose intensity relative to the planned dose intensity of each drug.



AIMS Press

©2020 the Author(s), licensee AIMS Press. This is an open access article distributed under the terms of the Creative Commons Attribution License (<http://creativecommons.org/licenses/by/4.0>)